Kinetics of light-induced degradation in semi-transparent perovskite solar cells

Jihoo Lim [a],[1], Moonyong Kim [a],[1], Helen Hejin Park [b], Hyunmin Jung [b], Sean Lim [c], Xiaojing Hao [a], Eunyoung Choi [a], Sangwook Park [a], Minwoo Lee [a], Ziheng Liu [a], Martin A. Green [a], Jangwon Seo [b], Jongsung Park [d], Jae Sung Yun [a],[*]

[a] *Australian Centre for Advanced Photovoltaics (ACAP), School of Photovoltaic and Renewable and Engineering, University of New South Wales, Sydney, NSW, 2052, Australia*
[b] *Advanced Materials Division, Korea Research Institute of Chemical Technology (KRICT), Daejeon, 34114, Republic of Korea*
[c] *Electron Microscope Unit, University of New South Wales, Sydney, NSW, 2052, Australia*
[d] *Solar Energy R&D Department, Green Energy Institute, Mokpo, Chonnam, 58656, Republic of Korea*

ARTICLE INFO

ABSTRACT

Perovskite solar cells (PSCs) have now achieved power conversion efficiencies (PCEs) over 25%, but their long-term stability under illumination and thermal stress is still a major barrier to commercialisation. Herein, we demonstrate the evaluation of light-induced degradation activation energy (E_a) of encapsulated semi-transparent PSCs by using the commonly employed method in crystalline silicon solar cells. Different parameters showed different activation energies where primary degradation is due to increase in series resistance, which also led to reduction in short-circuit current. Open-circuit voltage and shunt resistance also change with different E_a, suggesting the mechanism of the reduction is likely to be due to different reasons. Despite each parameter exhibiting slight variation over time for each temperature, the overall trend converges, indicating that each parameter is likely to be primarily reduced by a single dominant reaction. We also report the main cause of irreversible device degradation is not due to the decomposition of the perovskite layer as confirmed by X-ray diffraction characterisation. Instead, our pole figure map and absorption spectra analysis indicate that a loss of crystal symmetry occurs due to ion migration within the device that induce oxidation of 2,2′,7,7′-tetrakis-(*N,N*-di-4-methoxyphenylamino)-9,9′-spirobifluorene (Spiro-OMeTAD). Our work provides a better understanding through quantification of the degradation processes of encapsulated semi-transparent PSCs over time, which is essential for further progress and development of stable perovskite-Si tandem solar cells.

In the past ten years, mixed organic-inorganic halide perovskite solar cell (PSC) devices have attracted enormous attention due to their outstanding optoelectronic properties such as strong absorption, long carrier diffusion length, high carrier mobility and potentially low fabrication cost [1,2]. Power conversion efficiencies (PCEs) of PSC devices have increased impressively from 3.8% [3] to 25.2% [4] over a decade, reinforcing the promise for photovoltaic application [5,6]. Inspiringly, perovskite/silicon tandem solar cells have recently reached an efficiency of 29.15% [7], showing perovskite's huge potential for commercialisation through combining with the market-dominating silicon PV technology.

A recent study performed by Qian et al. showed that in order to compete with the future dominating passivated emitter and rear cell (PERC) technology, 30% efficient perovskite/silicon tandem solar cells require an annual degradation rate of <2% over 25 years [8]. PSCs currently have limitations in passing the International Electrotechnical Commission (IEC) standards designed for crystalline silicon solar cells [9–13]. So far, only a limited number of IEC tests have been passed such as IEC61215:2016 damp heat test [14,15] and IEC61215:2016 Humidity Freeze test [16].

The degradation and stability of the perovskite thin films and PSCs under various environmental stresses such as exposure to moisture [17–19], elevated temperature [20–22] and illumination [11,12,23] have been extensively studied. The degradations of PSCs are well known

to be caused by methylammonium iodide egress [21,24], moisture ingress [25,26], metal diffusion into hole transporting layer (HTL) [10, 27] and corrosion of metal electrodes by reaction with halides in the perovskite [28,29]. Many reports showed that the perovskite devices are more prone to be degraded resulting in irreversible device performance loss in J_{SC} and FF when they are exposed to both light and heat compared to being only exposed to thermal stress [10,27,29]. In particular, devices employing Spiro-OMeTAD as the HTL suffer from iodide ion migration [30], excessive photo-oxidation [31], causing volatile product formation such as HI gas [31], and metal diffusion [27] which results in voids forming in Spiro-OMeTAD [29,30] under illumination and heat.

Some of these degradation processes, however can be suppressed by encapsulating the PSCs, enhancing the long-term stability [32–34]. Therefore, considering that all commercialised photovoltaic modules are encapsulated with glass, or ethylene-vinyl acetate (EVA) and multilayer polymeric backsheets [35], some of those reactions may not be critical in the encapsulated PSCs due to containment of volatile species such as HI, CH_3NH_3, and CH_3Br [16]. Also, most of the above studies were performed with a single junction or an opaque device configuration, which only allow illumination by light from the glass side as the other side is fully covered by a metal electrode. Therefore, some of these observations may not be relevant to the degradation processes of potential tandem solar cells that consist of bifacial or semi-transparent PSCs.

In crystalline silicon solar cells (CSSCs), the thermal activation energy (E_a) of relevant reactions to light-induced degradation (LID) has been often utilised to evaluate long-term stability and operational lifetime [36]. Boron-oxygen related LID (BO-LID) [37] is a common example. While it is known to have fast and slow time-scale degradation components, the E_a for the temporary recovery in the dark [36,37] or for the degradation has been reported by analysing the reaction rate constants at different temperatures. The E_a values can be used for modelling long-term stability [38]. Moreover, the symmetrical result at different temperatures with different results can also imply a single reaction is induced during the controlled condition [36].

In contrast, even though there are many studies reporting on the ion migration activation energy ($E_{a,ion}$) within PSCs [39–41], there were no sufficient studies in investigating the E_a that has been employed for CSSCs. Only one study has used the approach to investigate E_a of the reactions in opaque PSCs [42]. However, the study reported E_a was based on the PCEs. While it can be used for estimation, since the change in PCEs can be attributed by all parameters, which include short-circuit current density (J_{SC}), open-circuit voltage (V_{OC}), series resistance (R_s) and the shunt resistance (R_{sh}), the value may have less physical meaning. In this paper, we demonstrate the E_a of change in different parameters due to LID using encapsulated semi-transparent PSCs. This study is the first report to analyse the temperature dependence of LID in semi-transparent PSCs. Further, we investigate the causes of the degradation using X-ray diffraction (XRD) pole figure mapping and absorption spectra.

Fig. 1 shows the semi-transparent PSC structure used in this study and the photocurrent density versus voltage (J-V) plots under 1-sun illumination. The semi-transparent mixed-cation PSC structures are AR film/Glass/ITO/SnO$_2$/FA$_{0.95}$MA$_{0.05}$Pb(I$_{0.95}$,Br$_{0.05}$)$_3$/Spiro-OMeTAD/MoO$_x$/ITO/Au/LiF as represented in Fig. 1 (a). The average values of the photovoltaic parameters for both forward and reverse bias scans measured at aperture areas of 0.3 cm^2 are shown in the inset of Fig. 1 (b).

The normalised values of the parameters of the encapsulated semi-transparent PSCs as a function of light-heat soaking time (t) at different light soaking temperatures (T) are shown in Fig. 2. For R_s and R_{sh}, the log values were used. The x-axis is in log scale, which can display the changes that may occur in different orders of magnitude over the light soaking time.

I–V curves for each temperature over time are summarised in Fig. S1, Supplementary Information. For all parameters, increasing T increased
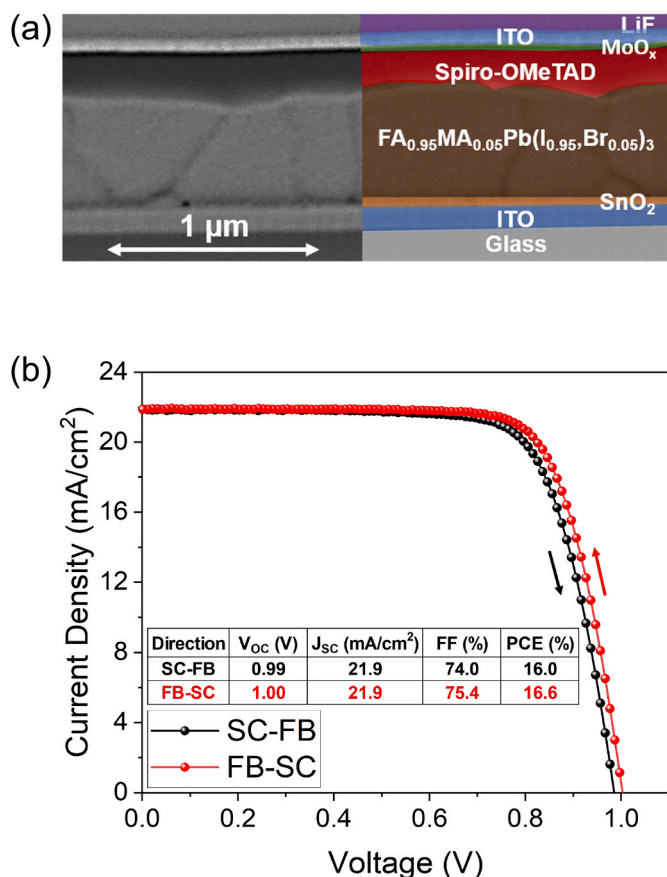

Fig. 1. (a) Cross-sectional Transmission Electron Microscope (TEM) image of a semi-transparent perovskite solar cell device configuration and (b) current density-voltage curves from short circuit to forward bias (SC-FB, black) and forward bias to short circuit (FB-SC, red) for the fresh device.

the rates of degradation. In particular, R_s and V_{OC} show approximately two and one order of magnitudes faster reaction, respectively, from 55 °C to 70 °C. Solid lines for each T for each parameter are fitted curve using Eq. (1).

$$i(t) = A \times exp(-k_{D,i}t) + y_0 \qquad [1]$$

Most of the fitted curves exhibit close agreement with measurements. While it is unclear in what order chemical reactions occur, the reaction rate constants can still be approximated based on the fittings.

The loss due to different parameters is known to be due to different reactions. The V_{OC} loss is likely due to the increased charge carrier recombination [43] and the charge carrier recombination rate is found to be increased with T, which leads to a reduction in the charge density within the perovskite layer [44], and thereby reduces V_{OC}. The drop in R_{sh} over time may be due to the loss of photocurrent through carrier recombination within the interfacial layers of the device caused by the non-radiative recombination losses [45]. The increase in R_s is known to be linked to the thermal stress [33,46] or interface degradation [47] where light may also accelerate the degradation reaction [48]. The J_{SC} loss could be caused by a reduction of charge carrier extraction efficiency [49] although due to the significant increase in R_s, it may have reduced the J_{SC}. For R_s, the initial stages (from 10 min to 1000 min) at 40 °C and 55 °C showed a slight increase and decrease before a significant improvement. However, at 70 °C primarily a single exponential increase in R_s is observed. It is unclear whether the changes in the early stages at 40 °C and 55 °C are dependent or independent to the other reactions. It appears to be that the reaction occurred at a similar time frame although the reaction superposed with the dominant reaction of
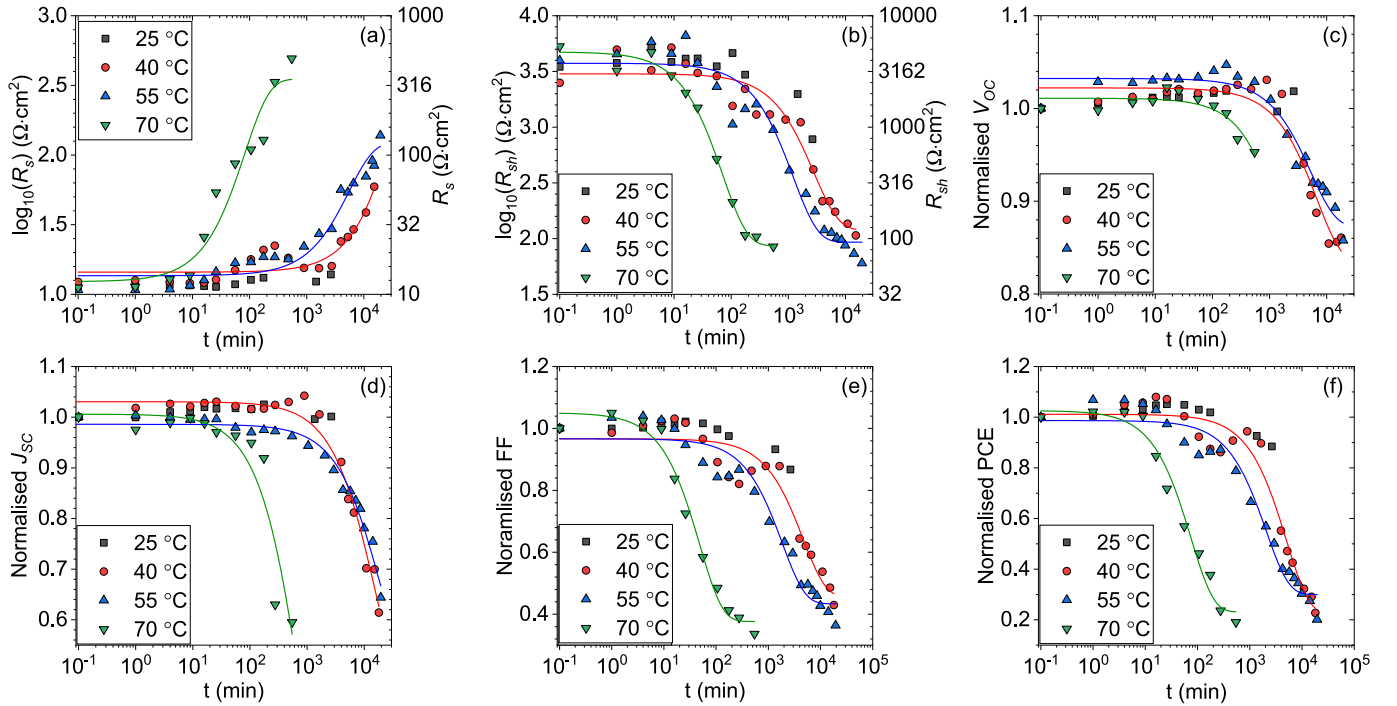
Fig. 2. Normalised device performance (Reverse I–V scan): (a) $\log_{10}(R_s)$, (b) $\log_{10}(R_{sh})$, (c) V_{OC}, (d) J_{SC}, (e) FF, and (f) PCE as a function of light-heat soaking time.

R_s increase. We will further investigate the possible cause of the reactions later in this work.

The degradation rate constant ($k_{D,i}$) as a function of $1/T$ for each photovoltaic parameter are shown in Fig. 3. Since the degradation at 25 °C was not significant, the result from the temperature was not included to estimate $E_{-a,i}$. The plots were then fitted using Eq. 2:

$$\ln\left(k_{D,i}\right) = A \times \exp\left(\frac{-E_{a,i}}{k_B T}\right), \qquad [2]$$

where $E_{a,i}$ is the E_a of parameter i and A is a pre-factor. The $E_{a,i}$ from the fitting can be found in Table 1. Higher $E_{a,i}$ indicates the reaction requires more thermal energy to occur and can be more susceptible changes with an increase in T. V_{OC} is directly related to the recombination behaviour of the perovskite absorber layer. As can be seen from XRD results (See Fig. S2, Supplementary Information), the perovskite layer did not decompose to PbI_2 under the light and heat soaking experiment.

Table 1
The thermal activation energy ($E_{a,i}$) for different parameters V_{OC}, J_{SC}, FF, PCE, R_s and R_{sh}.

Parameter (i)	$E_{a,i}$ (eV)
V_{OC}	0.15 ± 0.01
J_{SC}	1.59 ± 0.20
FF	1.39 ± 0.52
PCE	1.29 ± 0.46
R_s	2.04 ± 0.42
R_{sh}	1.17 ± 0.03

Therefore, it is likely that the V_{OC} has not been severely affected due to the loss of the perovskite absorber layer. Thus, the $E_{a,i}$ of V_{OC} shows the lowest which means that V_{OC} is less susceptible for changes with an increase in T. Note that the $E_{a,i}$ from PCE and FF have less physical meanings by themselves as they were influenced by more than one parameters.

To further investigate whether the reduction in each parameter is occurring by multiple or single reactions, Fig. 2 for each i are replotted as a function of normalised t respect to the $k_{D,i}$ as shown in Fig. 4. From Fig. 4 (a), (e), and (f), the trends for R_s, PCE and FF are similar, which both have a bump for the devices degraded under illumination at 40 °C and 55 °C between $k_{D,i}t$ is from 10^{-2} to 10^{-1}. While there is slight variation in the short time-frame ($k_{D,i}t$ from 10^{-2} to 10^{-1}), the overlap of the curves at longer time-frame, indicates the dominant reactions are due to a single reaction for each parameter.

This suggests that the primary cause of the reduction in both PCE and FF are due to the dominant increase in R_s. The I–V curves over time at each temperature (Fig. S1, Supplementary Information) display the main loss is due to R_s, while J_{SC} does not have a similar trend. However, considering the reduction in J_{SC} due to increase in R_s is expected when R_s is significantly high (generally above 200 $\Omega \cdot cm^2$), it is still likely that the reduction in J_{SC} is mainly responsible from R_s. The drop in R_{sh} can, however, still influence the $E_{a,i}$ of FF such that it may explain the $E_{a,i}$ based on FF is lower than R_s.

In addition, we observe no notable recovery after storing the devices in the dark for 12 h after measuring our last datapoint (~324 h of light
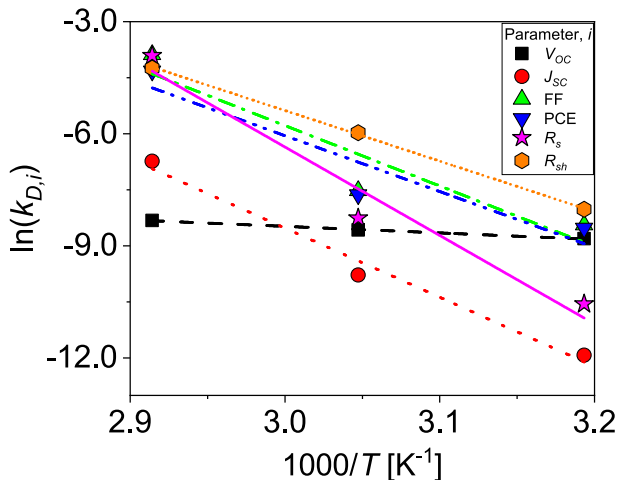

Fig. 3. Log value of reaction rate constants, $k_{D,i}$ for different parameters (i) as a function of inverse temperature (T).
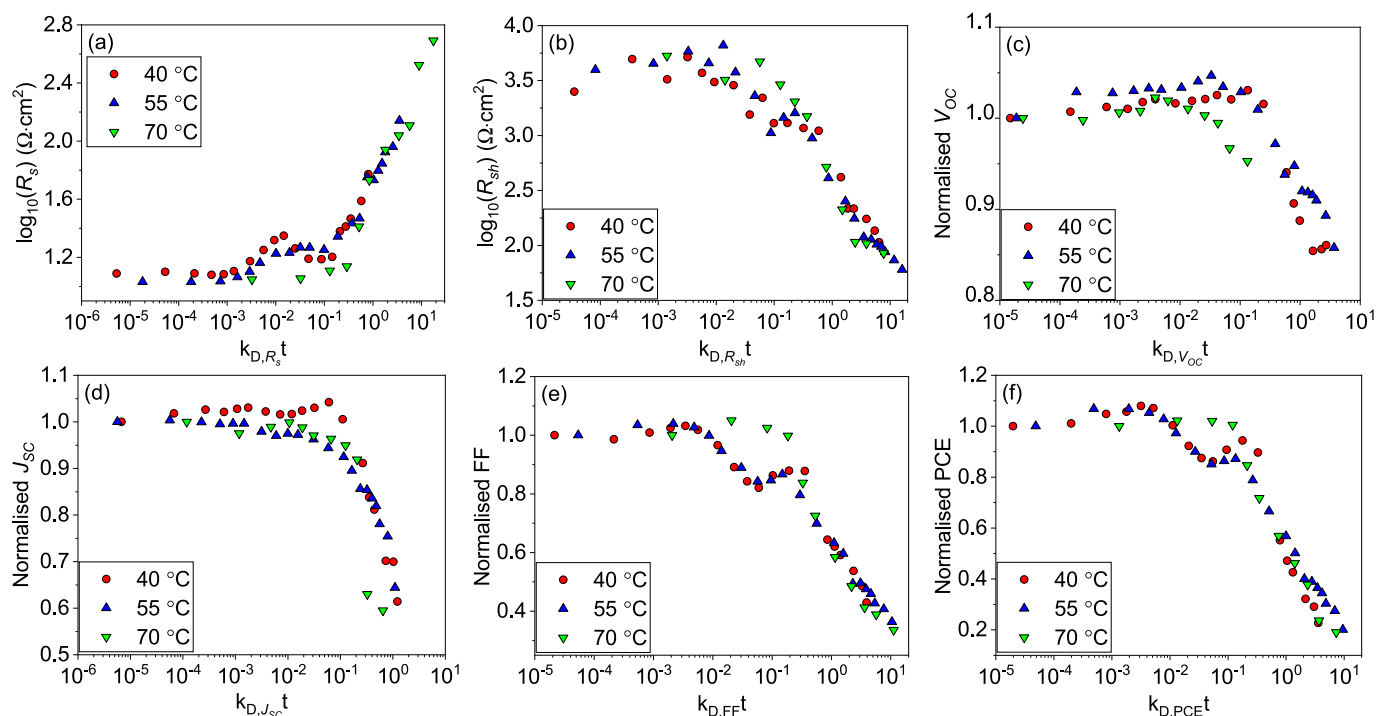
Fig. 4. Normalised device performance: (a) $\log_{10}(R_s)$, (b) $\log_{10}(R_{sh})$, (c) V_{OC}, (d) J_{SC}, (e) FF, and (f) PCE as a function of normalised light-heat soaking time.

soaking at 55 °C as an example), which suggests that such dominant reactions result in irreversible degradation (see Fig. S3, Supplementary Information).

While it is unclear whether the reduction in J_{SC} and increase in R_s are linked, the $E_{a,i}$ of R_{sh} and V_{OC} were different (1.17 eV and 0.15 eV, respectively) from the $E_{a,i}$ from R_s. Therefore, it is likely that the loss in those parameters is due to different reactions.

We measured XRD patterns of $FA_{0.95}MA_{0.05}Pb(I_{0.95}Br_{0.05})_3$, before and after illumination and thermal stress at 25 °C, 40 °C, 55 °C, and 70 °C (Fig. S2, Supplementary Information). The $FA_{0.95}MA_{0.05}Pb(I_{0.95}Br_{0.05})_3$ has two main perovskite peaks at 14.0° and 28.2° which are indexed to the (110) and (220) planes, respectively. The XRD measurements that were done at the end of the light-heat soaking experiment at different temperatures showed no significant peak of PbI_2. For encapsulated semi-transparent PSCs, we speculate that the egress of methylammonium iodide has been prevented by the ITO capping layer and the moisture ingress to the perovskite layer has also reduced by MoO_x buffer layer [50]. The result is in agreement with the literature which the degradation process and formation of PbI_2 were strongly suppressed by the introduction of a capping layer [24].

The XRD pole figure maps of from the sample without light soaking and with light soaking at 70 °C for 9.1 h are obtained and displayed in Fig. 5 (a) and (b) respectively. We chose the (110) planes as reference Bragg planes and map all of the (110) plane crystallites' orientation in the 3D space. It can be seen that there is a strong peak around the centre or normal direction, which implies that most of the crystals are oriented along the normal direction with small misorientation angles. On the other hand, the degraded sample exhibits reduced peak intensity at the centre, see Fig. 5 (b). XRD pole figure map of the subtraction of the intensities is exhibited in Fig. 5 (c). It can be clearly seen that the intensities are severely reduced around the centre. Also, small intensities are indiscriminately distributed throughout different directions. This implies that there are many crystals with high angle misorientations for the degraded sample. Fig. 5 (d) shows radial average intensity from each pole figure plotted as a function of Psi. The peak values of the samples with light soaking at 70 °C and without light soaking (control) were (3.6 $\pm$ 0.4) $\times 10^3$ and (1.5 $\pm$ 1.0) $\times 10^3$, respectively, which showed more

than a half reduction around the centre. As can be seen in the inset graph in Fig. 5 (d), the intensities also decrease when Psi is from 0° to 60°. Further, the intensities of the degraded sample have increased when Psi is from 65° to 85° which implies that the crystals have been significantly tilted – Fig. 5 (e) and (f) are schematic illustration of the (110) crystals of the fresh and degraded sample respectively. The perovskite did not completely decompose into PbI_2, but we speculate that a crystal symmetry is severely lost which could be attributed to escaping of halides from the perovskite layer due to heat and light stimulation [51].

Fig. 6 (a) shows that the absorption spectra after exposing the device under illumination at each T (25 °C, 40 °C, 55 °C, and 70 °C) including the fresh device. The absorption at 350–550 nm and at 600–900 nm decreases and increases, respectively, with higher T. The decrease in absorption at 350–550 nm resembles the spectra of the reaction of I^- ions with the Spiro-OMeTAD layer [52]. The increase in T can accelerate the migration of I^- ions [30] and hence there is more decrease in absorption with higher T. In order to improve the hole conductivity of Spiro-OMeTAD, the partial oxidation is required. Despite the increase in absorption at 600–900 nm, which is attributed to the oxidation of Spiro-OMeTAD [53,54], the excessive oxidation can result in poor device performance of PSCs [55]. Hence, the oxidation degree of Spiro-OMeTAD is critical as the oxidised Spiro-OMeTAD can improve the hole conductivity and thus enhance the efficiency of PSCs in a short-term, less than 30 min of continuous illumination, whereas excessive oxidation (more than 30 min) can result in low device performance [56].

However, the band edge of the degraded samples remains unchanged which indicate that the perovskite material is not decomposed into PbI_2 as suggested by the above XRD results. Fig. 6 (b) displays cross-sectional scanning electron microscope (SEM) images for samples milled in a focused-ion-beam (FIB), both for a fresh device and for a device degraded at 70 °C. As can be seen, the degraded sample does not show any sign of decomposition of the perovskite layer which is consistent with the XRD measurements (Fig.S2, Supplementary Information). However, voids were formed in the Spiro-OMeTAD layer of the degraded sample, particularly, above the grain boundaries of the perovskite layer which are marked in yellow circles. As suggested above, halide defects
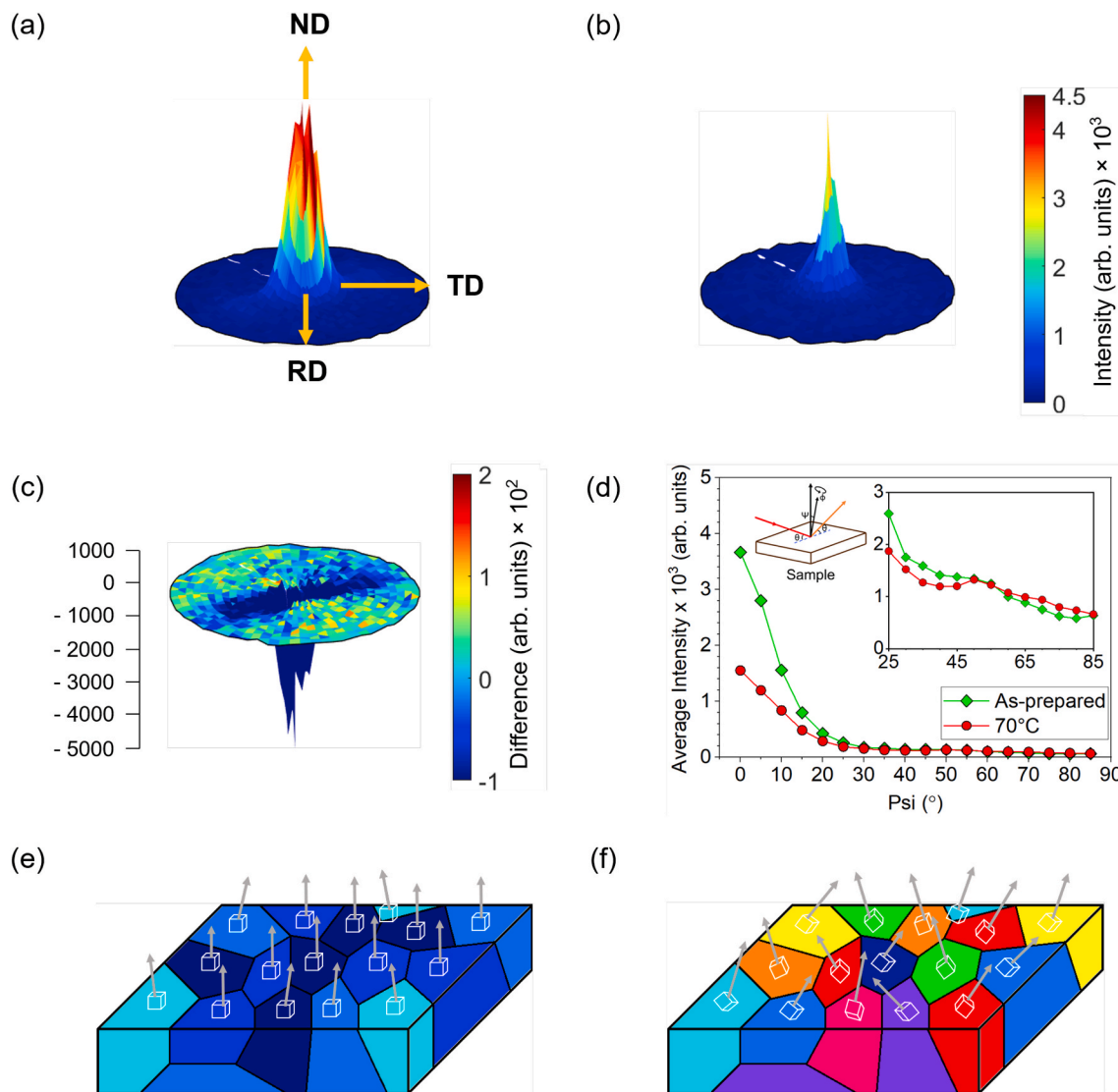
Fig. 5. X-ray diffraction pole figure maps of a (110) plane of (a) fresh and (b) degraded device under 1-sun illumination at 70 °C. ND, RD and TD represent normal direction, rolling direction and transverse direction, respectively, within the plane. The (110) direction ($2\theta = 14.0°$) defines the surface-normal direction, (c) XRD pole figure map of subtraction of intensities from fresh to 70 °C, and, (d) average intensity of pole figure map of fresh and degraded devices as a function of Psi (Ψ). The inset shows rotation angles (Φ, Ψ) of the (110) crystal planes. Illustration of crystals of the perovskite grains of (e) fresh and (f) degraded device.

form which are mobile. These mobile ions can easily diffuse through the grain boundaries [57], especially under heat and light, and react with Spiro-OMeTAD that results in a oxidation of Spiro-OMeTAD layer [54]. In particular, there are many studies reported that iodide (I^-) ions are more easily diffused from the perovskite layer to Spiro-OMeTAD [29,30] due to its lower migration activation energy compared to that of MA^+ and Pb^{2+} ions [39,40].

This can be further investigated by time-of-flight secondary ion mass spectrometry (ToF-SIMS) measurement. (See Fig. S4 in Supplementary Information). The depth profile of the fresh device and the device degraded at 70 °C is compared in Fig. S4 (a). The CN^- ion comes from either the Spiro-OMeTAD layer or the perovskite. I^- is ejected from the perovskite layer. We clearly see that more I^- ions have diffused into Spiro-OMeTAD, where CN^- intensity peaks at sputter time from 100 to 150 s, compared to fresh device as shown in the inset. In addition, the elemental 3D maps shown in Fig.S4 (b) shows the diffusion of I^- ions into the Spiro-OMeTAD. The iodide ions can easily react with oxidised Spiro-OMeTAD$^+$ which results in chemically reduced Spiro-OMeTAD [30] and thus the loss of hole transporting material conductivity and poor device performance [53].

In addition, the device performance may not only be affected by the intrinsic ion migration mentioned above but also the extrinsic ion migration such as Li^+ where it diffuses to both the hole transport layer and electron transport layer for devices employing Li-doped Spiro-OMeTAD [58]. Spiro-OMeTAD is well known to be prone to crystallisation under temperatures above 60 °C [59]. However, our XRD measurement (Fig. S2, Supplementary Information) exhibit no new peaks that are related to the crystalline phase of Spiro-OMeTAD which are indexed to 5.5°, 5.86°, 6.08°, and 12.16° [59] for the degraded devices, indicating there is no formation of crystallised Spiro-OMeTAD or the formed crystallised fine grain Spiro-OMeTAD is beyond the XRD detection limit.

In order to observe the effect of diffusion of ions to the Spiro-OMeTAD, the degraded sample is scanned in the reverse bias direction under illumination to revert the halide ions to back to the perovskite layer [39]. Fig. 6 (c) shows the absorption spectra of the sample degraded at 40 °C for 303.6 h after each reverse scan. It can be seen that the absorption at 350–550 nm gradually increases at each successive scan. This recovery of the absorption accompanies the recovery of the series resistance, which is shown in Fig. 6 (d).
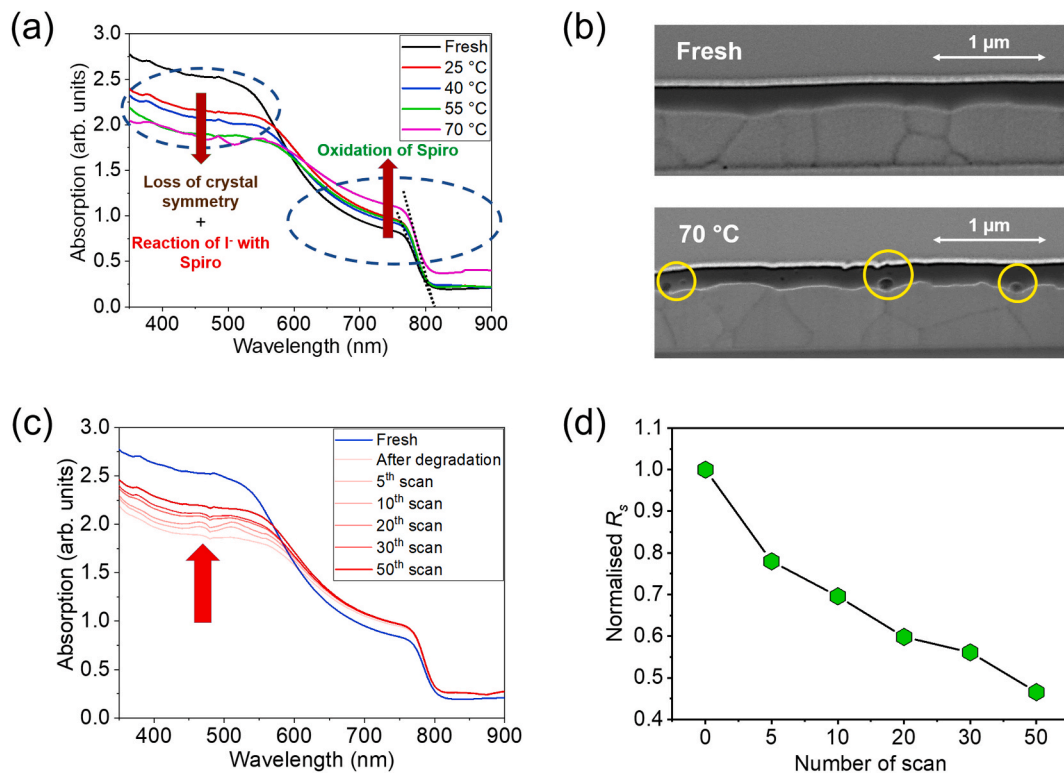
Fig. 6. (a) UV–vis absorption spectra of the fresh device and the degraded device under illumination at each temperature, (b) FIB-assisted cross-sectional SEM images of (top) fresh device and (bottom) the device degraded under illumination at 70 °C where yellow circles represent the voids formed in the Spiro-OMeTAD at the end of the grain boundaries, (c) Absorption measured before and after degrading the device under illumination at 40 °C and (d) Normalised R_s as a function of the number of I–V scans.

More importantly, based on Fig. 6 (a), it can be seen that the oxidation and I^- diffusion (voids formation in the Spiro-OMeTAD) simultaneously occur during the degradation process, thus, we think that both affects the increase in R_s of Spiro-OMeTAD layer, hence, degrade PSCs. It is not clear which dominates but from the recovery effect shown in Fig. 6 (c), the oxidation effect could not be recovered while the I^- diffusion can be partially recovered. Moreover, the oxidised Spiro-OMeTAD$^+$ is known to be neutrally bonded with I^- ion (Spiro-OMeTAD – I) [53]. This may also explain the absorption at 350–500 nm to be not recovered completely. Therefore, we think that the excessive oxidation of the Spiro-OMeTAD and the subsequent neutralised bonding reaction could be more critical in terms of permanent degradation of the PSCs.

In addition, in order to prove that the single reaction is likely due to the damage of Spiro-OMeTAD layer which dominates the complete degradation process, we removed the degraded Spiro-OMeTAD layer from the device degraded at 70 °C for 9.1 h and re-deposited a new Spiro-OMeTAD layer (See Fig. S5, Supplementary Information). We confirmed that the performance of the PSC has almost recovered (15.8% – 92.2% of its initial PCE) after redepositing the Spiro-OMeTAD (See Table S1), which indicates that the damage of Spiro-OMeTAD layer is critical in light-heat induced degradation.

Conclusion

In this study, the kinetics of light-induced degradation (LID) in semi-transparent perovskite solar cells (PSCs) are investigated. The primary loss of PCEs in PSCs was due to an increase in R_s, which led to a drop in J_{SC}. The $E_{a,i}$ of V_{OC} and R_{sh} were different from the $E_{a,i}$ of J_{SC} and R_s suggesting that the LID was likely to be due to different reactions. Moreover, for each parameter, the time normalised results showed close agreement that the primarily degradations are likely to be due to a single

reaction. Furthermore, XRD results showed the absence of PbI_2, which implies the perovskite layer was relatively stable within the tested stress range. However, XRD pole figure map results indicated that the crystallinity of the degraded perovskite layer was greatly reduced, possibly due to the creation of uncoordinated halide ions. Voids were formed in the Spiro-OMeTAD of the degraded device, particularly along the grain boundaries, which suggests that the ions diffused along the grain boundaries. Absorption spectra of the degraded sample exhibit the same behaviour to that of the oxidation of Spiro-OMeTAD. By reverting the diffused ions back to the perovskite, we confirm that the oxidation of Spiro-OMeTAD is partially recovered along with the series resistance. Our results highlight the significance of ion migration and series resistance in the degradation mechanism of encapsulated semi-transparent PSCs.

CRediT authorship contribution statement

Jihoo Lim: Writing - original draft, Writing - review & editing, Investigation, Visualization. **Moonyong Kim:** Conceptualization, Methodology, Writing - original draft. **Helen Hejin Park:** Resources, Writing - review & editing. **Hyunmin Jung:** Resources. **Sean Lim:** Investigation. **Xiaojing Hao:** Writing - review & editing. **Eunyoung Choi:** Validation, Writing - review & editing. **Sangwook Park:** Writing - review & editing. **Minwoo Lee:** Visualization, Writing - review & editing. **Ziheng Liu:** Writing - review & editing. **Martin A. Green:** Writing - review & editing. **Jangwon Seo:** Resources. **Jongsung Park:** Funding acquisition, Writing - review & editing. **Jae Sung Yun:** Supervision, Writing - review & editing, Writing - original draft.

Declaration of competing interest

The authors declare that they have no known competing financial

interests or personal relationships that could have appeared to influence the work reported in this paper.

Acknowledgement

Appendix A. Supplementary data

Supplementary data related to this article can be found at https ://doi.org/10.1016/j.solmat.2020.110776.

References

[1] S.D. Stranks, G.E. Eperon, G. Grancini, C. Menelaou, M.J.P. Alcocer, T. Leijtens, L. M. Herz, A. Petrozza, H.J. Snaith, Electron-hole diffusion lengths exceeding 1 micrometer in an organometal trihalide perovskite absorber, Science 342 (2013) 341.

[2] J.H. Noh, S.H. Im, J.H. Heo, T.N. Mandal, S.I. Seok, Chemical management for colorful, efficient, and stable inorganic–organic hybrid nanostructured solar cells, Nano Lett. 13 (2013) 1764–1769.

[3] A. Kojima, K. Teshima, Y. Shirai, T. Miyasaka, Organometal halide perovskites as visible-light sensitizers for photovoltaic cells, J. Am. Chem. Soc. 131 (2009) 6050–6051.

[4] NREL, Best Research-Cell Efficiency Chart, 2020.

[5] M.A. Green, A. Ho-Baillie, H.J. Snaith, The emergence of perovskite solar cells, Nat. Photon. 8 (2014) 506–514.

[6] M.A. Green, A. Ho-Baillie, Perovskite solar cells: the birth of a new era in photovoltaics, ACS Energy Letters 2 (2017) 822–830.

[7] H.Z. Berlin, World Record: Efficiency of Perovskite Silicon Tandem Solar Cell Jumps to 29.15 Per Cent, in, 2020.

[8] J. Qian, M. Ernst, N. Wu, A. Blakers, Impact of perovskite solar cell degradation on the lifetime energy yield and economic viability of perovskite/silicon tandem modules, Sustainable Energy & Fuels 3 (2019) 1439–1447.

[9] Y. Rong, Y. Hu, A. Mei, H. Tan, M.I. Saidaminov, S.I. Seok, M.D. McGehee, E. H. Sargent, H. Han, Challenges for commercializing perovskite solar cells, Science 361 (2018), eaat8235.

[10] T. Duong, Y. Wu, H. Shen, J. Peng, S. Zhao, N. Wu, M. Lockrey, T. White, K. Weber, K. Catchpole, Light and elevated temperature induced degradation (LeTID) in perovskite solar cells and development of stable semi-transparent cells, Sol. Energy Mater. Sol. Cell. 188 (2018) 27–36.

[11] D. Bryant, N. Aristidou, S. Pont, I. Sanchez-Molina, T. Chotchunangatchaval, S. Wheeler, J.R. Durrant, S.A. Haque, Light and oxygen induced degradation limits the operational stability of methylammonium lead triiodide perovskite solar cells, Energy Environ. Sci. 9 (2016) 1655–1660.

[12] J. Kim, J.S. Yun, Y. Cho, D.S. Lee, B. Wilkinson, A.M. Soufiani, X. Deng, J. Zheng, A. Shi, S.J.A.E.L. Lim, Overcoming the Challenges of Large-Area High-Efficiency Perovskite Solar Cells, vol. 2, 2017, pp. 1978–1984.

[13] W. Nie, J.-C. Blancon, A.J. Neukirch, K. Appavoo, H. Tsai, M. Chhowalla, M. A. Alam, M.Y. Sfeir, C. Katan, J. Even, S. Tretiak, J.J. Crochet, G. Gupta, A. D. Mohite, Light-activated photocurrent degradation and self-healing in perovskite solar cells, Nat. Commun. 7 (2016) 11574.

[14] K.A. Bush, A.F. Palmstrom, Z.J. Yu, M. Boccard, R. Cheacharoen, J.P. Mailoa, D. P. McMeekin, R.L.Z. Hoye, C.D. Bailie, T. Leijtens, I.M. Peters, M.C. Minichetti, N. Rolston, R. Prasanna, S. Sofia, D. Harwood, W. Ma, F. Moghadam, H.J. Snaith, T. Buonassisi, Z.C. Holman, S.F. Bent, M.D. McGehee, 23.6%-efficient monolithic perovskite/silicon tandem solar cells with improved stability, Nature Energy 2 (2017) 17009.

[15] C.C. Boyd, R. Cheacharoen, K.A. Bush, R. Prasanna, T. Leijtens, M.D. McGehee, Barrier design to prevent metal-induced degradation and improve thermal stability in perovskite solar cells, ACS Energy Letters 3 (2018) 1772–1778.

[16] L. Shi, M.P. Bucknall, T.L. Young, M. Zhang, L. Hu, J. Bing, D.S. Lee, J. Kim, T. Wu, N. Takamure, D.R. McKenzie, S. Huang, M.A. Green, A.W.Y. Ho-Baillie, Gas chromatography–mass spectrometry analyses of encapsulated stable perovskite solar cells, Science (2020), eaba2412.

[17] J.S. Yun, J. Kim, T. Young, R.J. Patterson, D. Kim, J. Seidel, S. Lim, M.A. Green, S. Huang, A. Ho-Baillie, Humidity-induced degradation via grain boundaries of HC (NH2)2PbI3 planar perovskite solar cells, Adv. Funct. Mater. 28 (2018) 1705363.

[18] J. Yang, B.D. Siempelkamp, D. Liu, T.L. Kelly, Investigation of CH3NH3PbI3 degradation rates and mechanisms in controlled humidity environments using in situ techniques, ACS Nano 9 (2015) 1955–1963.

[19] Q. Wang, B. Chen, Y. Liu, Y. Deng, Y. Bai, Q. Dong, J. Huang, Scaling behavior of moisture-induced grain degradation in polycrystalline hybrid perovskite thin films, Energy Environ. Sci. 10 (2017) 516–522.

[20] G. Divitini, S. Cacovich, F. Matteocci, L. Cinà, A. Di Carlo, C. Ducati, In situ observation of heat-induced degradation of perovskite solar cells, Nature Energy 1 (2016) 15012.

[21] B. Conings, J. Drijkoningen, N. Gauquelin, A. Babayigit, J. D'Haen, L. D'Olieslaeger, A. Ethirajan, J. Verbeeck, J. Manca, E. Mosconi, F.D. Angelis, H.-G. Boyen, Intrinsic thermal instability of methylammonium lead trihalide perovskite, Advanced Energy Materials 5 (2015), 1500477.

[22] N.-K. Kim, Y.H. Min, S. Noh, E. Cho, G. Jeong, M. Joo, S.-W. Ahn, J.S. Lee, S. Kim, K. Ihm, H. Ahn, Y. Kang, H.-S. Lee, D. Kim, Investigation of thermally induced degradation in CH3NH3PbI3 perovskite solar cells using in-situ synchrotron radiation analysis, Sci. Rep. 7 (2017) 4645.

[23] T. Leijtens, G.E. Eperon, S. Pathak, A. Abate, M.M. Lee, H.J. Snaith, Overcoming ultraviolet light instability of sensitized TiO2 with meso-superstructured organometal tri-halide perovskite solar cells, Nat. Commun. 4 (2013) 2885.

[24] K.A. Bush, C.D. Bailie, Y. Chen, A.R. Bowring, W. Wang, W. Ma, T. Leijtens, F. Moghadam, M.D. McGehee, Thermal and environmental stability of semi-transparent perovskite solar cells for tandems enabled by a solution-processed nanoparticle buffer layer and sputtered ITO electrode, Adv. Mater. 28 (2016) 3937–3943.

[25] S.N. Habisreutinger, T. Leijtens, G.E. Eperon, S.D. Stranks, R.J. Nicholas, H. J. Snaith, Carbon nanotube/polymer composites as a highly stable hole collection layer in perovskite solar cells, Nano Lett. 14 (2014) 5561–5568.

[26] T. Leijtens, T. Giovenzana, S.N. Habisreutinger, J.S. Tinkham, N.K. Noel, B. A. Kamino, G. Sadoughi, A. Sellinger, H.J. Snaith, Hydrophobic organic hole transporters for improved moisture resistance in metal halide perovskite solar cells, ACS Appl. Mater. Interfaces 8 (2016) 5981–5989.

[27] K. Domanski, J.-P. Correa-Baena, N. Mine, M.K. Nazeeruddin, A. Abate, M. Saliba, W. Tress, A. Hagfeldt, M. Grätzel, Not all that glitters is gold: metal-migration-induced degradation in perovskite solar cells, ACS Nano 10 (2016) 6306–6314.

[28] Y. Kato, L.K. Ono, M.V. Lee, S. Wang, S.R. Raga, Y. Qi, Silver iodide formation in methyl ammonium lead iodide perovskite solar cells with silver top electrodes, Advanced Materials Interfaces 2 (2015), 1500195.

[29] Y. Han, S. Meyer, Y. Dkhissi, K. Weber, J.M. Pringle, U. Bach, L. Spiccia, Y.-B. Cheng, Degradation observations of encapsulated planar CH3NH3PbI3 perovskite solar cells at high temperatures and humidity, J. Mater. Chem. 3 (2015) 8139–8147.

[30] S. Kim, S. Bae, S.-W. Lee, K. Cho, K.D. Lee, H. Kim, S. Park, G. Kwon, S.-W. Ahn, H.-M. Lee, Y. Kang, H.-S. Lee, D. Kim, Relationship between ion migration and interfacial degradation of CH3NH3PbI3 perovskite solar cells under thermal conditions, Sci. Rep. 7 (2017) 1200.

[31] Y. Zhao, W. Zhou, H. Tan, R. Fu, Q. Li, F. Lin, D. Yu, G. Walters, E.H. Sargent, Q. Zhao, Mobile-ion-induced degradation of organic hole-selective layers in perovskite solar cells, J. Phys. Chem. C 121 (2017) 14517–14523.

[32] T. Leijtens, G.E. Eperon, N.K. Noel, S.N. Habisreutinger, A. Petrozza, H.J. Snaith, Stability of metal halide perovskite solar cells, Advanced Energy Materials 5 (2015), 1500963.

[33] F. Matteocci, L. Cinà, E. Lamanna, S. Cacovich, G. Divitini, P.A. Midgley, C. Ducati, A. Di Carlo, Encapsulation for long-term stability enhancement of perovskite solar cells, Nanomater. Energy 30 (2016) 162–172.

[34] H.C. Weerasinghe, Y. Dkhissi, A.D. Scully, R.A. Caruso, Y.-B. Cheng, Encapsulation for improving the lifetime of flexible perovskite solar cells, Nanomater. Energy 18 (2015) 118–125.

[35] C. Wiesmeier, I. Haedrich, K.-A. Weiss, I. Duerr, Overview of PV module encapsulation materials, Photovoltaics International 19 (2013) 85–92.

[36] M. Kim, M. Abbott, N. Nampalli, S. Wenham, B. Stefani, B. Hallam, Modulating the extent of fast and slow boron-oxygen related degradation in Czochralski silicon by thermal annealing: evidence of a single defect, J. Appl. Phys. 121 (2017), 053106.

[37] K. Bothe, J. Schmidt, Electronically activated boron-oxygen-related recombination centers in crystalline silicon, J. Appl. Phys. 99 (2006), 013701.

[38] A.M. Ciesla, J.I. Bilbao, C.E. Chan, D.N.R. Payne, D. Chen, M. Kim, S.R. Wenham, B.J. Hallam, Modeling boron–oxygen degradation and self-repairing silicon PV modules in the field, IEEE Journal of Photovoltaics 10 (2020) 28–40.

[39] C. Eames, J.M. Frost, P.R.F. Barnes, B.C. O'Regan, A. Walsh, M.S. Islam, Ionic transport in hybrid lead iodide perovskite solar cells, Nat. Commun. 6 (2015) 7497.

[40] J.M. Azpiroz, E. Mosconi, J. Bisquert, F. De Angelis, Defect migration in methylammonium lead iodide and its role in perovskite solar cell operation, Energy Environ. Sci. 8 (2015) 2118–2127.

[41] J. Haruyama, K. Sodeyama, L. Han, Y. Tateyama, First-principles study of ion diffusion in perovskite solar cell sensitizers, J. Am. Chem. Soc. 137 (2015) 10048–10051.

[42] J. Kim, N. Park, J.S. Yun, S. Huang, M.A. Green, A.W.Y. Ho-Baillie, An effective method of predicting perovskite solar cell lifetime–Case study on planar CH3NH3PbI3 and HC(NH2)2PbI3 perovskite solar cells and hole transfer materials of spiro-OMeTAD and PTAA, Sol. Energy Mater. Sol. Cell. 162 (2017) 41–46.

[43] T. Leijtens, G.E. Eperon, A.J. Barker, G. Grancini, W. Zhang, J.M. Ball, A.R. S. Kandada, H.J. Snaith, A. Petrozza, Carrier trapping and recombination: the role of defect physics in enhancing the open circuit voltage of metal halide perovskite solar cells, Energy Environ. Sci. 9 (2016) 3472–3481.

[44] E.J. Juarez-Perez, M. Wußler, F. Fabregat-Santiago, K. Lakus-Wollny, E. Mankel, T. Mayer, W. Jaegermann, I. Mora-Sero, Role of the selective contacts in the

performance of lead halide perovskite solar cells, J. Phys. Chem. Lett. 5 (2014) 680–685.

[45] D. Luo, R. Su, W. Zhang, Q. Gong, R. Zhu, Minimizing non-radiative recombination losses in perovskite solar cells, Nature Reviews Materials 5 (2020) 44–60.

[46] Q. Wang, C. Bi, J. Huang, Doped hole transport layer for efficiency enhancement in planar heterojunction organolead trihalide perovskite solar cells, Nanomater. Energy 15 (2015) 275–280.

[47] A. Guerrero, J. You, C. Aranda, Y.S. Kang, G. Garcia-Belmonte, H. Zhou, J. Bisquert, Y. Yang, Interfacial degradation of planar lead halide perovskite solar cells, ACS Nano 10 (2016) 218–224.

[48] G. Abdelmageed, C. Mackeen, K. Hellier, L. Jewell, L. Seymour, M. Tingwald, F. Bridges, J.Z. Zhang, S. Carter, Effect of temperature on light induced degradation in methylammonium lead iodide perovskite thin films and solar cells, Sol. Energy Mater. Sol. Cell. 174 (2018) 566–571.

[49] W. Tress, N. Marinova, T. Moehl, S.M. Zakeeruddin, M.K. Nazeeruddin, M. Grätzel, Understanding the rate-dependent J–V hysteresis, slow time component, and aging in CH3NH3PbI3 perovskite solar cells: the role of a compensated electric field, Energy Environ. Sci. 8 (2015) 995–1004.

[50] E.M. Sanehira, B.J. Tremolet de Villers, P. Schulz, M.O. Reese, S. Ferrere, K. Zhu, L. Y. Lin, J.J. Berry, J.M. Luther, Influence of electrode interfaces on the stability of perovskite solar cells: reduced degradation using MoOx/Al for hole collection, ACS Energy Letters 1 (2016) 38–45.

[51] G.Y. Kim, A. Senocrate, T.-Y. Yang, G. Gregori, M. Grätzel, J.J.N.m. Maier, in: Large Tunable Photoeffect on Ion Conduction in Halide Perovskites and Implications for Photodecomposition, vol. 17, 2018, pp. 445–449.

[52] J. Carrillo, A. Guerrero, S. Rahimnejad, O. Almora, I. Zarazua, E. Mas-Marza, J. Bisquert, G. Garcia-Belmonte, Ionic reactivity at contacts and aging of

methylammonium lead triiodide perovskite solar cells, Advanced Energy Materials 6 (2016), 1502246.

[53] R.S. Sanchez, E. Mas-Marza, Light-induced effects on Spiro-OMeTAD films and hybrid lead halide perovskite solar cells, Sol. Energy Mater. Sol. Cell. 158 (2016) 189–194.

[54] G. Liu, L. Liu, X. Niu, H. Zhou, Q. Chen, Effects of iodine doping on carrier behavior at the interface of perovskite crystals: efficiency and stability, MD 8 (2018).

[55] X. Wang, J. Wu, Y. Yang, X. Liu, Q. Guo, Z. Song, G. Li, Z. Lan, M. Huang, High performance and stable perovskite solar cells using vanadic oxide as a dopant for spiro-OMeTAD, J. Mater. Chem. 7 (2019) 13256–13264.

[56] S. Wang, W. Yuan, Y.S. Meng, Spectrum-dependent spiro-OMeTAD oxidization mechanism in perovskite solar cells, ACS Appl. Mater. Interfaces 7 (2015) 24791–24798.

[57] J.S. Yun, J. Seidel, J. Kim, A.M. Soufiani, S. Huang, J. Lau, N.J. Jeon, S.I. Seok, M. A. Green, A. Ho-Baillie, Critical role of grain boundaries for ion migration in formamidinium and methylammonium lead halide perovskite solar cells, Advanced Energy Materials 6 (2016), 1600330.

[58] Z. Li, C. Xiao, Y. Yang, S.P. Harvey, D.H. Kim, J.A. Christians, M. Yang, P. Schulz, S. U. Nanayakkara, C.-S. Jiang, J.M. Luther, J.J. Berry, M.C. Beard, M.M. Al-Jassim, K. Zhu, Extrinsic ion migration in perovskite solar cells, Energy Environ. Sci. 10 (2017) 1234–1242.

[59] T. Malinauskas, D. Tomkute-Luksiene, R. Sens, M. Daskeviciene, R. Send, H. Wonneberger, V. Jankauskas, I. Bruder, V. Getautis, Enhancing thermal stability and lifetime of solid-state dye-sensitized solar cells via molecular engineering of the hole-transporting material spiro-OMeTAD, ACS Appl. Mater. Interfaces 7 (2015) 11107–11116.